 CMES, vol.120, no. 1, pp. 105-121, 2019

Modelling and Backstepping Motion Control of the Aircraft Skin Inspection Robot

Junjun Jiang[1] and Congqing Wang[1, *]

Abstract: Aircraft skin health concerns whether the aircraft can fly safely. In this paper, an improved mechanical structure of the aircraft skin inspection robot was introduced. Considering that the aircraft skin surface is a curved environment, we assume that the curved environment is equivalent to an inclined plane with a change in inclination. Based on this assumption, the Cartesian dynamics model of the robot is established using the Lagrange method. In order to control the robot's movement position accurately, a position backstepping control scheme for the aircraft skin inspection robot was presented. According to the dynamic model and taking into account the problems faced by the robot during its movement, a position constrained controller of the aircraft skin inspection robot is designed using the barrier Lyapunov function. Aiming at the disturbances in the robot, we adopt a fuzzy system to approximate the unknown dynamics related with system states. Finally, the simulation results of the designed position constrained controller were compared with the sliding mode controller, and prove the validity of the position constrained controller.

Keywords: Aircraft skin inspection robot, dynamics modelling, backstepping control, fuzzy system, barrier lyapunov function, motion control.

1 Introduction

Today, the health inspection of the aircraft skin is mainly done by humans. The inspection efficiency is low, the assessment of the test results is not standard, and it is greatly affected by human factors. A variety of wall-climbing robots are designed to accomplish some tasks. In Apostolescu et al. [Apostolescu, Alexandrescu, Ionascu et al. (2011)], a climbing robot using the electro-pneumatically vacuum cups was designed. In Miyake et al. [Miyake, Ishihara, Shoji et al. (2006)], a small-size and light weight window cleaning robot was developed, the prototype robot consists of two driven wheels and an active suction cup. In Nagakubo et al. [Nagakubo and Hirose (1994)], a kind of wall climbing robot was designed with a gecko-like structure by observing the gecko climbing wall behavior. In Rosa et al. [Rosa, Messina, Muscato et al. (2002)], a type of low-cost climbing robot was proposed which can climb cylindrical painted iron surfaces using eight suction cups, the robot carries an ultrasonic probe equipment to evaluate the integrity of the metal in the inspection of storage tanks.

[1] College of Automation Engineering, Nanjing University of Aeronautics and Astronautics, Nanjing, China.

[*] Corresponding Author: Congqing Wang. Email: cqwang@nuaa.edu.cn.

In order to solve the problems of suction and motion for wall-climbing robots, many useful control strategies have been proposed. In Wettach et al. [Wettach, Hillenbrand and Berns (2006)], the basic thermodynamic model was presented, which was necessary to describe the changes of the pressure under robot motion condition. Based on this model, a controller of vacuum chambers was designed to adjust the chambers pressure. In Yong et al. [Yong, Wang, Fang et al. (2007)], based on the multiple-model adaptive estimation and the Boolean logic reasoning, an approach to fault detection and identification in suction foot control of a climbing robot was presented. In Zhang et al. [Zhang, Zhang and Zong (2008)], a new pneumatic climbing robot was presented to satisfy the requirements of glass-wall cleaning. Furthermore, a segment and variable bang-bang controller was developed to implement the precise control of the position servo system for the X cylinder during the sideways movement. In He et al. [He, Li, and Chen (2017)], a comprehensive survey of the recent development of the human-centered intelligent robot was provided, and the issues and challenges in the field were discussed.

In recent years, researches on intelligent control strategies of robots under input or output constrains have been conducted in-depth. In He et al. [He, Ge, Li et al. (2017); He, Dong and Sun (2015)], some control strategies for some articulated robots and affine nonlinear systems were designed when the systems are subjected to external disturbances and output constraint. In Chen et al. [Chen, Ge and Ren (2011)], an adaptive tracking control method was proposed for a class uncertain multiple input and multiple output nonlinear systems with input constraint. In Ren et al. [Ren, Ge, Tee et al. (2010)], aiming at output feedback nonlinear systems in the presence of unknown functions, a class of control strategies were presented by using adaptive neural network and Backstepping technique. In Li et al. [Li, Li and Jing (2014)], a novel indirect adaptive fuzzy controller for a class of uncertain nonlinear systems with input and output constrains was proposed by using a barrier Lyapunov function and an auxiliary design system to solve input and output constraints. In Chen et al. [Chen, Ge, and How (2010)], the author proposed a robust adaptive neural network control strategy for a class of uncertain multi-input and multi-output nonlinear systems with input nonlinearities. Niu et al. [Niu and Zhao (2013); Niu, Liu, Zong et al. (2017)] investigated the control strategies under output constraint for switching systems and time-varying output constraint system. Ngo et al. [Ngo, Mahony and Jiang (2005); Li, Li, Liu et al. (2017)] dealt with a class of control problems for nonlinear multi-input and multi-output systems with full state constraints.

In this paper, we mainly study the motion control of the inspection robot on the surface of the aircraft skin. Considering the chattering in the sliding mode controller, the robot movement is restricted by the work environment, on the one hand the chattering will cause a violent change in the robot’s adsorption force, which will lead to the drastic change of the robot's adsorption force and cause the robot to fall off because of the lack of enough adsorption force. On the other hand, the inaccurate position control of the robot can cause the robot legs touch the surface of the aircraft skin, and then affect the normal motion of the robot. It may cause the robot breaks down or slides directly from the surface of the plane. So we must avoid the robot legs touching the surface of the aircraft skin. Inspired by the above researches, we design a position controller based on the backstepping control with output constraint.

This paper is organized as follows. Section 2 describes the structure of the aircraft skin inspection robot, and Section 3 analyzes the dynamics of the inspection robot. In Section 4, the backstepping control method of the robot is designed by using a barrier Lyapunov function, and the fuzzy system-based adaptive method is used to approximate the unknown dynamics related with system states. Then, the stability of the closed-loop of the robot system is proved by the constructed Lyapunov function. Simulation results are given in Section 5.

2 The structure of the aircraft skin inspection robot

The aircraft skin health inspection robot with dual-frame is shown in Fig. 1. The robot can absorb on the aircraft fuselage using negative pressure. The robot can provide a load of about 15Kg that is enough to support the body and keep stability during inspection. There are four layers in the robot‘s structure. The first and fourth layers of the robot are the outer frame and inner frame, two servomotors and a speed reducer are installed so that the two frames can rotate. The servomotor of the outer frame is used to drive the rotating movement of the inner frame, and the servomotor of the inner frame is used to drive the rotating movement of the outer frame. The second layer of the robot is a mechanism for the robot to achieve pitch attitude adjustment. The purpose is to enable the robot to adapt the surface curvature of the aircraft skin during movement. The third layer is the sliding layer of the robot. A sliding servomotor is used to drive the ball screw to generate translational motion. The inner and outer frames are respectively installed with four mechanical legs, and the legs are connected with vacuum suction cups, so that the robot can adsorb on the surface of the aircraft skin.

Figure 1: Aircraft skin inspection robot with double frame

3 Dynamic modelling

Fig. 2 gives an improved structure of the aircraft skin inspection robot with double frame. The following discussion will focus on the movement of the robot on an inclined plane with a dip angle α .

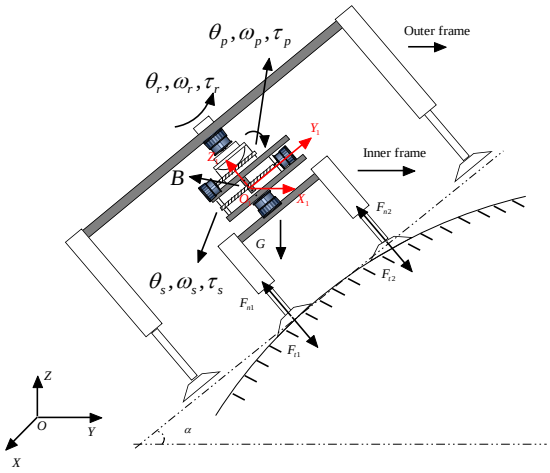

Figure 2: Structure of the robot

In Fig. 2, $O-XYZ$ is the global coordinate system, $O_1-X_1Y_1Z_1$ is the body coordination system. O_1 is selected at the point B of the robot. G is the gravity of the robot. Point A is selected as the reference point of position and velocity. r is the horizontal distance between point A and the rotation servomotor axis of the outer frame. r_1 is the distance from point A to the fixed end of the ball screw. τ_s is the torque of the sliding servomotor acting on the ball screw, w_s is the angular velocity of the motor driving the ball screw, and θ_s is the rotation angle of the ball screw. The rotation of the ball screw drives the horizontal movement of the sliding layer. τ_p is the torque produced by a pitch motor, ω_p is the angular velocity of the pitch motor, and the θ_p is the angle between inner frame and outer frame which is produced by the pitch motor, τ_r is the rotation torque produced by the rotating motor, ω_r is the rotational angular velocity, and the θ_r is the angle of rotation axis. F_{n1}, F_{n2} are the support forces. F_{t1}, F_{t2} are the absorption forces. The driving system of the robot is shown in Fig. 3.

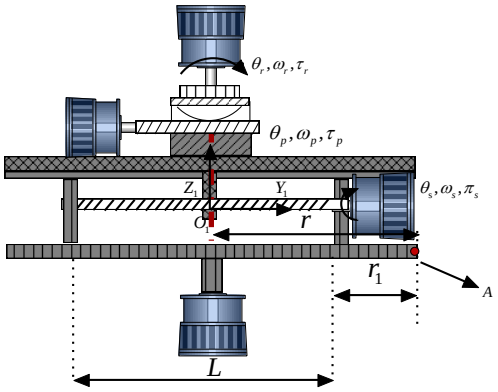

Figure 3: The driving system of the robot

3.1 Dynamic model in joint space

In Fig. 3, the moment of inertia of the inner frame is calculated by

$$I = \int_{r-2r_1-L}^{r} \lambda y_1^2 dy_1 \tag{1}$$

where I is the inertia of the inner frame , m_1 is the mass of the sliding motion body, L is total sliding distance, y_1 is the horizontal sliding distance of the inner frame, and λ is the equivalent mass density of the rigid body, which satisfies

$$m_1 = \lambda L \tag{2}$$

The kinetic model is derived by the Lagrange formula as follows:

Kinetic energy of the inner frame is

$$E_k = \frac{1}{2} m_1 \dot{r}^2 + \frac{1}{2} I \omega_r^2 = \frac{1}{2}\left(m_1 \left(k\dot{\theta}_s \right)^2 + I\dot{\theta}_r^2 \right) \tag{3}$$

where $r = k\theta_s$, k is the helical pitch of the ball screw.

The potential energy of the moving inner frame is

$$E_p = m_1 g \left(k\theta_s - r_1 \right) \sin\left(\alpha + \theta_p \right) \cos\theta_r \tag{4}$$

The Lagrange function of the inner frame can be written as:

$$\begin{aligned} L &= E_k - E_p \\ &= \frac{1}{2}\left(m_1 \left(k\dot{\theta}_s \right)^2 + I\dot{\theta}_r^2 \right) - m_1 g \left(k\theta_s - r_1 \right) \sin\left(\alpha + \theta_p \right) \cos\theta_r \end{aligned} \tag{5}$$

Therefore, the dynamics equation of the inner frame is given by:

$$\begin{cases} \tau_r = \dfrac{d}{dt}\dfrac{\partial L}{\partial \dot{\theta}_r} - \dfrac{\partial L}{\partial \theta_r} \\ \tau_s = \dfrac{d}{dt}\dfrac{\partial L}{\partial \dot{\theta}_s} - \dfrac{\partial L}{\partial \theta_s} \\ \tau_p = \dfrac{d}{dt}\dfrac{\partial L}{\partial \dot{\theta}_p} - \dfrac{\partial L}{\partial \theta_p} \end{cases} \tag{6}$$

We can obtain the dynamic equation of the inner frame in joint space as follows:

$$\boldsymbol{\tau} = \boldsymbol{M}(\boldsymbol{q})\ddot{\boldsymbol{q}} + \boldsymbol{C}(\boldsymbol{q},\dot{\boldsymbol{q}})\dot{\boldsymbol{q}} + \boldsymbol{G}(\boldsymbol{q}) \tag{7}$$

where $\boldsymbol{q} = \begin{bmatrix} q_1 & q_2 & q_3 \end{bmatrix}^T = \begin{bmatrix} \theta_r & \theta_s & \theta_p \end{bmatrix}^T$ is the vector of joint angles, $\boldsymbol{\tau} = \begin{bmatrix} \tau_r & \tau_s & \tau_p \end{bmatrix}^T$ is a vector of torques at the joints, $\boldsymbol{M}(\boldsymbol{q})$ is a mass matrix, $\boldsymbol{C}(\boldsymbol{q},\dot{\boldsymbol{q}})$ is a vector of centrifugal and Coriolis terms, and $\boldsymbol{G}(\boldsymbol{q})$ is a vector of gravity terms. $\boldsymbol{M}(\boldsymbol{q})$, $\boldsymbol{C}(\boldsymbol{q},\dot{\boldsymbol{q}})$ and $\boldsymbol{G}(\boldsymbol{q})$ are given by

$$\boldsymbol{M}(\boldsymbol{q})=\begin{bmatrix}\frac{\lambda}{3}\left[(k\theta_s)^3+\left(L-(k\theta_s)+2r_1\right)^3\right] & 0 & 0\\ 0 & m_1 & 0\\ 0 & 0 & \frac{\lambda}{3}\left[(k\theta_s)^3+\left(L-(k\theta_s)+2r_1\right)^3\right]\end{bmatrix},$$

$$\boldsymbol{C}(\boldsymbol{q},\dot{\boldsymbol{q}})=$$

$$\begin{bmatrix}\lambda\left[(k\theta_s)^2-\left(L-(k\theta_s)+2r_1\right)^2\right](k\dot{\theta}_s) & 0 & 0\\ 0 & -\frac{\lambda}{2}\left[(k\theta_s)^2-\left(L-(k\theta_s)+2r_1\right)^2\right]\dot{\theta}_r & -\frac{\lambda}{2}\left[(k\theta_s)^2-\left(L-(k\theta_s)+2r_1\right)^2\right]\dot{\theta}_p\\ 0 & 0 & -\lambda\left[(k\theta_s)^2-\left(L-(k\theta_s)+2r_1\right)^2\right]\dot{\theta}_r\end{bmatrix},$$

$$\boldsymbol{G}(\boldsymbol{q})=\begin{bmatrix}m_1 g\left(r_1-(k\theta_s)\right)\sin(\alpha+\theta_p)\sin\theta_r\\ m_1 g\sin(\alpha+\theta_p)\cos\theta_r\\ m_1 g\left(r_1-(k\theta_s)\right)\cos(\alpha+\theta_p)\cos\theta_r\end{bmatrix}.$$

3.2 Dynamic model in Cartesian space

In Fig. 3, the position of the point A in the coordinate system $O_1-X_1Y_1Z_1$ is expressed as:

$$\begin{cases}x_1=r\cos\theta_p\cos\theta_r\\ y_1=r\cos\theta_p\sin\theta_r\\ z_1=\sqrt{x_1^2+y_1^2}\tan\theta_p\end{cases}\tag{8}$$

From (8), we can obtain:

$$\begin{cases}r=\sqrt{x_1^2+y_1^2+z_1^2}\\ \theta_r=\arccos\dfrac{x_1}{\sqrt{x_1^2+y_1^2}}\\ \theta_p=\arctan\dfrac{z_1}{\sqrt{x_1^2+y_1^2}}\end{cases}$$

(9)

Define $\boldsymbol{x}=\begin{bmatrix}x_1 & y_1 & z_1\end{bmatrix}^T$, the transformation from joint velocity to Cartesian velocity is $d\boldsymbol{x}=Jd\boldsymbol{q}$,

where $\boldsymbol{J}=\dfrac{\partial \boldsymbol{x}}{\partial \boldsymbol{q}}$ is the Jacobian matrix, $\boldsymbol{J}=\begin{bmatrix} \dfrac{\partial x_1}{\partial q_1} & \dfrac{\partial x_1}{\partial q_2} & \dfrac{\partial x_1}{\partial q_3} \\ \dfrac{\partial y_1}{\partial q_1} & \dfrac{\partial y_1}{\partial q_2} & \dfrac{\partial y_1}{\partial q_3} \\ \dfrac{\partial z_1}{\partial q_1} & \dfrac{\partial z_1}{\partial q_2} & \dfrac{\partial z_1}{\partial q_3} \end{bmatrix}$.

According to the above relationship, we can obtain:

$$\boldsymbol{J}(\boldsymbol{q})=\begin{bmatrix} -k\theta_s \sin\theta_r \cos\theta_p & \cos\theta_r \cos\theta_p & -k\theta_s \sin\theta_p \cos\theta_r \\ k\theta_s \cos\theta_p \cos\theta_r & \cos\theta_p \sin\theta_r & -k\theta_s \sin\theta_p \sin\theta_r \\ 0 & \sin\theta_p & k\theta_s \cos\theta_p \end{bmatrix} \tag{10}$$

where the range of θ_p is set as $\theta_p \in \left[-60^\circ, 60^\circ\right]$ such that the Jacobian matrix is full rank.

In the Cartesian space, when the Jacobian matrix is full rank, the virtual control force $\boldsymbol{F}_x=\left[F_r, F_s, F_p\right]^T$ is expressed as

$$\boldsymbol{F}_x = \boldsymbol{J}^{-T}(\boldsymbol{q})\boldsymbol{\tau} \tag{11}$$

Since $\dot{\boldsymbol{x}} = \boldsymbol{J}\dot{\boldsymbol{q}}$, we can obtain:

$$\dot{\boldsymbol{q}} = \boldsymbol{J}^{-1}(\boldsymbol{q})\dot{\boldsymbol{x}} \tag{12}$$

From Eq. (12), we can obtain:

$$\ddot{\boldsymbol{x}} = \dot{\boldsymbol{J}}(\boldsymbol{q})\dot{\boldsymbol{q}} + \boldsymbol{J}(\boldsymbol{q})\ddot{\boldsymbol{q}} = \dot{\boldsymbol{J}}(\boldsymbol{q})\boldsymbol{J}^{-1}(\boldsymbol{q})\dot{\boldsymbol{x}} + \boldsymbol{J}(\boldsymbol{q})\ddot{\boldsymbol{q}} \tag{13}$$

According to Eq. (12) and Eq. (13), we can obtain:

$$\ddot{\boldsymbol{q}} = \boldsymbol{J}^{-1}(\boldsymbol{q})\left(\ddot{\boldsymbol{x}} - \dot{\boldsymbol{J}}(\boldsymbol{q})\boldsymbol{J}^{-1}(\boldsymbol{q})\dot{\boldsymbol{x}}\right) \tag{14}$$

Substituting Eq. (12) and Eq. (14) into Eq. (7), we can obtain:

$$\boldsymbol{\tau} = \boldsymbol{M}(\boldsymbol{q})\boldsymbol{J}^{-1}(\boldsymbol{q})\left(\ddot{\boldsymbol{x}} - \dot{\boldsymbol{J}}(\boldsymbol{q})\boldsymbol{J}^{-1}(\boldsymbol{q})\dot{\boldsymbol{x}}\right) + \boldsymbol{C}(\boldsymbol{q},\dot{\boldsymbol{q}})\boldsymbol{J}^{-1}(\boldsymbol{q})\dot{\boldsymbol{x}} + \boldsymbol{G}(\boldsymbol{q}) \tag{15}$$

Then, Eq. (15) can be expressed as:

$$\boldsymbol{\tau} = \boldsymbol{M}(\boldsymbol{q})\boldsymbol{J}^{-1}(\boldsymbol{q})\ddot{\boldsymbol{x}} + \left(\boldsymbol{C}(\boldsymbol{q},\dot{\boldsymbol{q}}) - \boldsymbol{M}(\boldsymbol{q})\boldsymbol{J}^{-1}(\boldsymbol{q})\dot{\boldsymbol{J}}(\boldsymbol{q})\right)\boldsymbol{J}^{-1}(\boldsymbol{q})\dot{\boldsymbol{x}} + \boldsymbol{G}(\boldsymbol{q}) \tag{16}$$

Multiplying both sides of (15) by $\boldsymbol{J}^{-T}(\boldsymbol{q})$ yields

$$\boldsymbol{J}^{-T}(\boldsymbol{q})\boldsymbol{\tau} = \boldsymbol{J}^{-T}(\boldsymbol{q})\left(\boldsymbol{M}(\boldsymbol{q})\boldsymbol{J}^{-1}(\boldsymbol{q})\ddot{\boldsymbol{x}} + \left(\boldsymbol{C}(\boldsymbol{q},\dot{\boldsymbol{q}}) - \boldsymbol{M}(\boldsymbol{q})\boldsymbol{J}^{-1}(\boldsymbol{q})\dot{\boldsymbol{J}}(\boldsymbol{q})\right)\boldsymbol{J}^{-1}(\boldsymbol{q})\dot{\boldsymbol{x}} + \boldsymbol{G}(\boldsymbol{q})\right) \tag{17}$$

According to Eq. (11) and considering the disturbance, we can obtain the following Cartesian dynamics model.

$$\boldsymbol{F}_x = \boldsymbol{M}_x(\boldsymbol{q})\ddot{\boldsymbol{x}} + \boldsymbol{C}_x(\boldsymbol{q},\dot{\boldsymbol{q}})\dot{\boldsymbol{x}} + \boldsymbol{G}_x(\boldsymbol{q}) + \boldsymbol{f}_{dis}(t) + \boldsymbol{F}_f(\dot{\boldsymbol{q}}) \tag{18}$$

where

$\boldsymbol{M}_x(\boldsymbol{q}) = \boldsymbol{J}^{-T}(\boldsymbol{q})\boldsymbol{M}(\boldsymbol{q})\boldsymbol{J}^{-1}(\boldsymbol{q})$ is the Cartesian inertia matrix,

$\boldsymbol{C}_x(\boldsymbol{q},\dot{\boldsymbol{q}}) = \boldsymbol{J}^{-T}(\boldsymbol{q})\left(\boldsymbol{C}(\boldsymbol{q},\dot{\boldsymbol{q}}) - \boldsymbol{M}(\boldsymbol{q})\boldsymbol{J}^{-1}(\boldsymbol{q})\dot{\boldsymbol{J}}(\boldsymbol{q})\right)\boldsymbol{J}^{-1}(\boldsymbol{q})$ is the Cartesian Coriolis/centripetal vector, $\boldsymbol{G}_x(\boldsymbol{q}) = \boldsymbol{J}^{-T}(\boldsymbol{q})\boldsymbol{G}(\boldsymbol{q})$ is the Cartesian gravity vector , $\boldsymbol{f}_{dis}$ is an unknown disturbance, and $\boldsymbol{F}_f$ is a friction force.

Assumption 1: $\boldsymbol{f}_{dis}(t)$ is continuous and uniformly bounded, there exists a constant D, such that $\left\| \boldsymbol{f}_{dis}(t) \right\| \le D, \forall t \in [0,\infty)$.

Eq. (18) has the following properties:

The property 1: $\boldsymbol{M}_x(\boldsymbol{q})$ is a positive definite symmetric matrix.

The property 2: $\dot{\boldsymbol{M}}_x(\boldsymbol{q}) - 2\boldsymbol{C}_x(\boldsymbol{q},\dot{\boldsymbol{q}})$ is a skew symmetric matrix.

4 Backstepping position controller design using barrier lyapunov function

Define $\boldsymbol{x}_1 = \boldsymbol{x} = \begin{bmatrix} x_1 & y_1 & z_1 \end{bmatrix}^T$, $\boldsymbol{x}_2 = \dot{\boldsymbol{x}}_1$.

Thus the dynamics model (18) can be transformed into a state-space expression as

$$\begin{cases} \dot{\boldsymbol{x}}_1 = \boldsymbol{x}_2 \\ \dot{\boldsymbol{x}}_2 = \boldsymbol{M}_x^{-1}(\boldsymbol{q})\left[\boldsymbol{F}_x - \boldsymbol{C}_x(\boldsymbol{q},\dot{\boldsymbol{q}})\dot{\boldsymbol{x}}_2 - \boldsymbol{G}_x(\boldsymbol{q}) - \boldsymbol{f}_{dis} - \boldsymbol{F}_f(\dot{\boldsymbol{q}})\right] \end{cases} \tag{19}$$

The robot position error is defined as:

$$\boldsymbol{e}_1 = \boldsymbol{x}_1 - \boldsymbol{x}_d \tag{20}$$

where $\boldsymbol{e}_1 = \begin{bmatrix} e_{11}, e_{12}, e_{13} \end{bmatrix}^T$, $\boldsymbol{x}_d$ is the desired position trajectory in Cartesian space.

The auxiliary variable error is defined as:

$$\boldsymbol{e}_2 = \boldsymbol{x}_2 - \boldsymbol{\alpha} \tag{21}$$

where $\boldsymbol{\alpha}$ is the virtual control.

The derivative of $\boldsymbol{e}_2$ is expressed as:

$$\dot{\boldsymbol{e}}_2 = \dot{\boldsymbol{x}}_2 - \dot{\boldsymbol{\alpha}} \tag{22}$$

where $\boldsymbol{e}_2 = \begin{bmatrix} e_{21}, e_{22}, e_{23} \end{bmatrix}^T$.

In order to ensure that the legs do not touch the aircraft skin during the motion of the robot, we adopt the barrier Lyapunov function to restrain the trajectory tracking error.

The barrier Lyapunov function is selected as follows:

$$V_1 = \frac{1}{2}\sum_{i=1}^{i=3} \ln \frac{b_i^2}{b_i^2 - e_{1i}^2} \tag{23}$$

where $b_i > 0$ is a small constant.

The derivative of V_1 is written as:

$$\dot{V}_1 = \sum_{i=1}^{i=3} \frac{e_{1i}\dot{e}_{1i}}{b_i^2 - e_{1i}^2} = \sum_{i=1}^{i=3} \frac{e_{1i}\left(e_{2i} + \alpha_i - \dot{x}_i\right)}{b_i^2 - e_{1i}^2} \tag{24}$$

The virtual control α_i is selected as follows:

$$\alpha_i = -k_i e_{1i} + \dot{x}_i \tag{25}$$

where $k_i > 0$.

Substituting Eq. (25) into Eq. (24) yields:

$$\begin{aligned} \dot{V}_1 &= \sum_{i=1}^{i=3} \frac{e_{1i}\left(e_{2i} + \alpha_i - \dot{x}_i\right)}{b_i^2 - e_{1i}^2} \\ &= -\sum_{i=1}^{i=3} \frac{k_i e_{1i}^2}{b_i^2 - e_{1i}^2} + \sum_{i=1}^{i=3} \frac{e_{1i} e_{2i}}{b_i^2 - e_{1i}^2} \end{aligned} \tag{26}$$

The second-order Lyapunov function is selected as

$$V_2 = V_1 + \frac{1}{2}\boldsymbol{e}_2^T \boldsymbol{M}_x(\boldsymbol{q})\boldsymbol{e}_2 \tag{27}$$

The derivative of V_2 is obtained as:

$$\dot{V}_2 = \dot{V}_1 + \boldsymbol{e}_2^T \boldsymbol{M}_x(\boldsymbol{q})\dot{\boldsymbol{e}}_2 + \frac{1}{2}\boldsymbol{e}_2^T \dot{\boldsymbol{M}}_x(\boldsymbol{q})\boldsymbol{e}_2 \tag{28}$$

Substituting Eq. (21) into Eq. (28), we can obtain:

$$\dot{V}_2 = \dot{V}_1 + \boldsymbol{e}_2^T \left(\boldsymbol{M}_x(\boldsymbol{q})(\dot{\boldsymbol{x}}_2 - \dot{\boldsymbol{\alpha}}) + \frac{1}{2}\dot{\boldsymbol{M}}_x(\boldsymbol{q})\boldsymbol{e}_2 \right) \tag{29}$$

Substituting Eq. (19) and Eq. (21) into Eq. (29) yields:

$$\dot{V}_2 = \dot{V}_1 + \boldsymbol{e}_2^T \left\{ \boldsymbol{F}_x - \boldsymbol{C}_x(\boldsymbol{q},\dot{\boldsymbol{q}})\boldsymbol{\alpha} - \boldsymbol{G}_x(\boldsymbol{q}) - \boldsymbol{f}_{dis} - \boldsymbol{F}_f(\dot{\boldsymbol{q}}) - \boldsymbol{M}_x(\boldsymbol{q})\dot{\boldsymbol{\alpha}} + \frac{1}{2}\left(\dot{\boldsymbol{M}}_x(\boldsymbol{q}) - 2\boldsymbol{C}_x(\boldsymbol{q},\dot{\boldsymbol{q}})\right)\boldsymbol{e}_2 \right\} \tag{30}$$

Based on the property 2 and Eq. (26), we can obtain:

$$\begin{aligned} \dot{V}_2 &= \dot{V}_1 + \boldsymbol{e}_2^T \left\{ \boldsymbol{F}_x - \boldsymbol{C}_x(\boldsymbol{q},\dot{\boldsymbol{q}})\boldsymbol{\alpha} - \boldsymbol{G}_x(\boldsymbol{q}) - \boldsymbol{f}_{dis} - \boldsymbol{F}_f(\dot{\boldsymbol{q}}) - \boldsymbol{M}_x(\boldsymbol{q})\dot{\boldsymbol{\alpha}} \right\} \\ &= -\sum_{i=1}^{i=3} \frac{k_i e_{1i}^2}{b_i^2 - e_{1i}^2} + \sum_{i=1}^{i=3} \frac{e_{1i} e_{2i}}{b_i^2 - e_{1i}^2} + \boldsymbol{e}_2^T \left\{ \boldsymbol{F}_x - \boldsymbol{C}_x(\boldsymbol{q},\dot{\boldsymbol{q}})\boldsymbol{\alpha} - \boldsymbol{G}_x(\boldsymbol{q}) - \boldsymbol{f}_{dis} - \boldsymbol{F}_f(\dot{\boldsymbol{q}}) - \boldsymbol{M}_x(\boldsymbol{q})\dot{\boldsymbol{\alpha}} \right\} \end{aligned} \tag{31}$$

Since the $\boldsymbol{C}_x(\boldsymbol{q},\dot{\boldsymbol{q}}), \boldsymbol{G}_x(\boldsymbol{q}), \boldsymbol{M}_x(\boldsymbol{q})$ cannot be accurately known, we adopt a fuzzy system to approximate the unknown dynamics related with system states.

Define $\boldsymbol{f} = -\boldsymbol{C}_x(\boldsymbol{q},\dot{\boldsymbol{q}})\boldsymbol{\alpha} - \boldsymbol{G}_x(\boldsymbol{q}) - \boldsymbol{M}_x(\boldsymbol{q})\dot{\boldsymbol{\alpha}} - \boldsymbol{F}_f(\dot{\boldsymbol{q}})$. A single-valued fuzzy, product inference engine and average defuzzification of the center of gravity are used for the nonlinear approximation. Fuzzy rule is expressed as:

If x_1 is F_1^j and … and x_n is F_n^j ,Then y is B^j . $j = 1, 2, ..., N$

where F_i^j and B^j are fuzzy sets of membership functions $\mu_{A_i^j}(x_i)$ and $\mu_{B^j}(y)$ respectively, N is the number of rules.

Then, the output of the fuzzy system can be defined as

$$y\left(\boldsymbol{x}_{fls}\right)=\frac{\sum_{j=1}^{N}\bar{y}_j\prod_{i=1}^{n}\mu_{F_i^j}\left(x_i\right)}{\sum_{j=1}^{N}\left[\prod_{i=1}^{n}\mu_{F_i^j}\left(x_i\right)\right]}=\boldsymbol{\xi}^T\left(\boldsymbol{x}_{fls}\right)\boldsymbol{\theta} \tag{32}$$

where $\boldsymbol{x}_{fls}=\left[x_1,x_2,...,x_n\right]^T\in R^n$, $\boldsymbol{\xi}\left(\boldsymbol{x}_{fls}\right)=\left[\xi_1\left(\boldsymbol{x}_{fls}\right),\xi_2\left(\boldsymbol{x}_{fls}\right),...,\xi_N\left(\boldsymbol{x}_{fls}\right)\right]^T$,

$\xi_j\left(\boldsymbol{x}_{fls}\right)=\dfrac{\prod_{i=1}^{n}\mu_{F_i^j}\left(x_i\right)}{\sum_{j=1}^{N}\left[\prod_{i=1}^{n}\mu_{F_i^j}\left(x_i\right)\right]}$, $\boldsymbol{\theta}=\left[\theta_1,\theta_2,...,\theta_N\right]^T=\left[\bar{y}_1,\bar{y}_2,...,\bar{y}_N\right]^T$, $\bar{y}_j=\max_{y\in R}\mu_{B^j}\left(y\right)$.

Based on the above method of the fuzzy system, the approximation of the unknown parameters can be designed as follows:

$$\boldsymbol{\Phi}=\boldsymbol{\xi}^T\left(\boldsymbol{x}_{fls}\right)\boldsymbol{\theta} \tag{33}$$

where $\boldsymbol{\Phi}=\left[\varphi_1\left(\boldsymbol{x}_{fls}\right)\quad\varphi_2\left(\boldsymbol{x}_{fls}\right)\quad\varphi_3\left(\boldsymbol{x}_{fls}\right)\right]^T$, $\boldsymbol{x}_{fls}=\left[\boldsymbol{x}_1^T,\boldsymbol{x}_2^T,\boldsymbol{\alpha}^T,\dot{\boldsymbol{\alpha}}^T\right]^T$,

$$\xi^T\left(\boldsymbol{x}_{fls}\right)=\begin{bmatrix}\xi_1^T\left(\boldsymbol{x}_{fls}\right)&0&0\\0&\xi_2^T\left(\boldsymbol{x}_{fls}\right)&0\\0&0&\xi_3^T\left(\boldsymbol{x}_{fls}\right)\end{bmatrix},\ \boldsymbol{\theta}=\begin{bmatrix}\boldsymbol{\theta}_1\\\boldsymbol{\theta}_2\\\boldsymbol{\theta}_3\end{bmatrix},\ \varphi_1\left(\boldsymbol{x}_{fls}\right)=\frac{\sum_{i=1}^{i=7}\theta_{1i}\prod_{j=1}^{j=12}\mu_{F_j^i}\left(x_j\right)}{\sum_{i=1}^{i=7}\left[\prod_{j=1}^{j=12}\mu_{F_j^i}\left(x_j\right)\right]}=\xi_1^T\left(\boldsymbol{x}_{fls}\right)\boldsymbol{\theta}_1,$$

$$\varphi_2\left(\boldsymbol{x}_{fls}\right)=\frac{\sum_{i=1}^{i=7}\theta_{2i}\prod_{j=1}^{j=12}\mu_{F_j^i}\left(x_j\right)}{\sum_{i=1}^{i=7}\left[\prod_{j=1}^{j=12}\mu_{F_j^i}\left(x_j\right)\right]}=\xi_2^T\left(\boldsymbol{x}_{fls}\right)\boldsymbol{\theta}_2,\ \varphi_3\left(\boldsymbol{x}_{fls}\right)=\frac{\sum_{i=1}^{i=7}\theta_{3i}\prod_{j=1}^{j=12}\mu_{F_j^i}\left(x_j\right)}{\sum_{i=1}^{i=7}\left[\prod_{j=1}^{j=12}\mu_{F_j^i}\left(x_j\right)\right]}=\xi_3^T\left(\boldsymbol{x}_{fls}\right)\boldsymbol{\theta}_3.$$

The membership function is selected as

$$\mu_{F_j^i}\left(x_j\right)=\exp\left(-0.5\left(\frac{x_j+1.5-0.5*(i-1)}{0.6}\right)^2\right)\left(i=1,2,3,...,7,\ j=1,2,3,...,12\right) \tag{34}$$

Define the optimal approximation parameter $\boldsymbol{\theta}^*$ and the optimal approximation $\boldsymbol{\Phi}^*$ for a given arbitrarily small constant $\varepsilon\left(\varepsilon>0\right)$, we have $\left\|\boldsymbol{f}-\boldsymbol{\Phi}^*\right\|\le\varepsilon$.

Then we design the controller as following

$$\boldsymbol{F}_x=-\boldsymbol{K}_2\boldsymbol{e}_2-\sum_{i=1}^{i=3}\frac{e_{1i}}{b_i^2-e_{1i}^2}-\boldsymbol{\Phi}-l\boldsymbol{e}_2 \tag{35}$$

where $\boldsymbol{K}_2>0$ is a diagonal matrix, $l>0$ is a constant.

Substituting Eq. (35) into Eq. (31), we can obtain

$$\dot{V}_2=-\sum_{i=1}^{i=3}\frac{k_ie_{1i}^2}{b_i^2-e_{1i}^2}-\boldsymbol{e}_2{}^TK_2\boldsymbol{e}_2+\boldsymbol{e}_2{}^T\left(\boldsymbol{f}-\boldsymbol{\Phi}\right)-e_2{}^Tl\boldsymbol{e}_2-e_2{}^T\boldsymbol{f}_{\boldsymbol{dis}} \tag{36}$$

Let $\tilde{\boldsymbol{\theta}}=\boldsymbol{\theta}^*-\boldsymbol{\theta}$, the corresponding adaptive parameter control law is designed:

$$\dot{\boldsymbol{\theta}}=\gamma\left(\boldsymbol{e}_2^T\xi^T\left(\boldsymbol{x}_{fls}\right)\right)^T-2a\boldsymbol{\theta} \tag{37}$$

Lyapunov function is selected as：

$$V_3 = V_2 + \frac{1}{2\gamma}\tilde{\boldsymbol{\theta}}^T\tilde{\boldsymbol{\theta}} \tag{38}$$

The derivative of V_3 is written as:

$$\dot{V}_3 = \dot{V}_2 - \frac{1}{\gamma}\tilde{\boldsymbol{\theta}}^T\dot{\boldsymbol{\theta}} \tag{39}$$

Substituting Eq. (36) into Eq. (39), we can obtain:

$$\begin{aligned}
\dot{V}_3 &= -\sum_{i=1}^{i=3}\frac{k_i e_{1i}^2}{b_i^2 - e_{1i}^2} - \boldsymbol{e}_2{}^T K_2\boldsymbol{e}_2 + \boldsymbol{e}_2{}^T(\boldsymbol{f} - \boldsymbol{\Phi}) - \frac{1}{\gamma}\tilde{\boldsymbol{\theta}}^T\dot{\boldsymbol{\theta}} - e_2{}^T l\boldsymbol{e}_2 - e_2{}^T\boldsymbol{f}_{\boldsymbol{dis}} \\
&\le -\sum_{i=1}^{i=3}\frac{k_i e_{1i}^2}{b_i^2 - e_{1i}^2} - \boldsymbol{e}_2{}^T K_2\boldsymbol{e}_2 + \boldsymbol{e}_2{}^T\left(\boldsymbol{f} - \boldsymbol{\xi}^T\left(\boldsymbol{x}_{fls}\right)\boldsymbol{\theta}\right) - \frac{1}{\gamma}\tilde{\boldsymbol{\theta}}^T\dot{\boldsymbol{\theta}} - e_2{}^T l\boldsymbol{e}_2 + le_2{}^T\boldsymbol{e}_2 + \frac{1}{4l}\left\|\boldsymbol{f}_{\boldsymbol{dis}}\right\|^2 \\
&\le -\sum_{i=1}^{i=3}\frac{k_i e_{1i}^2}{b_i^2 - e_{1i}^2} - \boldsymbol{e}_2{}^T K_2\boldsymbol{e}_2 + \boldsymbol{e}_2{}^T\left(\boldsymbol{f} - \boldsymbol{\xi}^T\left(\boldsymbol{x}_{fls}\right)\boldsymbol{\theta}^*\right) + e_2{}^T\left(\boldsymbol{\xi}^T\left(\boldsymbol{x}_{fls}\right)\boldsymbol{\theta}^* - \boldsymbol{\xi}^T\left(\boldsymbol{x}_{fls}\right)\boldsymbol{\theta}\right) - \frac{1}{\gamma}\tilde{\boldsymbol{\theta}}^T\dot{\boldsymbol{\theta}} + \frac{1}{4l}D^2 \\
&\le -\sum_{i=1}^{i=3}\frac{k_i e_{1i}^2}{b_i^2 - e_{1i}^2} - \boldsymbol{e}_2{}^T K_2\boldsymbol{e}_2 + \left\|\boldsymbol{e}_2{}^T\right\|\left\|\boldsymbol{f} - \boldsymbol{\xi}^T\left(\boldsymbol{x}_{fls}\right)\boldsymbol{\theta}^*\right\| + \boldsymbol{e}_2{}^T\left(\boldsymbol{\xi}^T\left(\boldsymbol{x}_{fls}\right)\tilde{\boldsymbol{\theta}}\right) - \frac{1}{\gamma}\tilde{\boldsymbol{\theta}}^T\dot{\boldsymbol{\theta}} + \frac{1}{4l}D^2 \\
&\le -\sum_{i=1}^{i=3}\frac{k_i e_{1i}^2}{b_i^2 - e_{1i}^2} - \boldsymbol{e}_2{}^T K_2\boldsymbol{e}_2 + \frac{1}{2}\left\|\boldsymbol{e}_2{}^T\right\|^2 + \frac{1}{2}\|\boldsymbol{\varepsilon}\|^2 + \tilde{\boldsymbol{\theta}}^T\left[\left(\boldsymbol{e}_2{}^T\boldsymbol{\xi}^T\left(\boldsymbol{x}_{fls}\right)\right)^T - \frac{1}{\gamma}\dot{\boldsymbol{\theta}}\right] + \frac{1}{4l}D^2
\end{aligned} \tag{40}$$

Substituting the adaptive parameter control law Eq. (37) into Eq. (40), we can obtain:

$$\begin{aligned}
\dot{V}_3 &\le -\sum_{i=1}^{i=3}\frac{k_i e_{1i}^2}{b_i^2 - e_{1i}^2} - \boldsymbol{e}_2{}^T K_2\boldsymbol{e}_2 + \frac{1}{2}\left\|\boldsymbol{e}_2{}^T\right\|^2 + \frac{1}{2}\|\boldsymbol{\varepsilon}\|^2 \\
&+ \tilde{\boldsymbol{\theta}}^T\left\{\left(e_2{}^T\boldsymbol{\xi}^T\left(\boldsymbol{x}_{fls}\right)\right)^T - \frac{1}{\gamma}\left[\gamma\left(\boldsymbol{e}_2^T\boldsymbol{\xi}^T\left(\boldsymbol{x}_{fls}\right)\right)^T - 2a\boldsymbol{\theta}\right]\right\} + \frac{1}{4l}D^2 \\
&= -\sum_{i=1}^{i=3}\frac{k_i e_{1i}^2}{b_i^2 - e_{1i}^2} - \boldsymbol{e}_2{}^T\left(K_2 - \frac{1}{2}I\right)\boldsymbol{e}_2 + \frac{a}{\gamma}\left(2\boldsymbol{\theta}^{*T}\boldsymbol{\theta} - 2\boldsymbol{\theta}^T\boldsymbol{\theta}\right) + \frac{1}{2}\|\boldsymbol{\varepsilon}\|^2 + \frac{1}{4l}D^2
\end{aligned} \tag{41}$$

Due to $\left(\boldsymbol{\theta} - \boldsymbol{\theta}^*\right)^T\left(\boldsymbol{\theta} - \boldsymbol{\theta}^*\right) = \boldsymbol{\theta}^T\boldsymbol{\theta} - 2\boldsymbol{\theta}^{*T}\boldsymbol{\theta} + \boldsymbol{\theta}^{*T}\boldsymbol{\theta}^* \ge 0$,we can obtain:

$$2\boldsymbol{\theta}^{*T}\boldsymbol{\theta} - 2\boldsymbol{\theta}^T\boldsymbol{\theta} \le -\boldsymbol{\theta}^T\boldsymbol{\theta} + \boldsymbol{\theta}^{*T}\boldsymbol{\theta}^* \tag{42}$$

Substituting the Eq. (42) into the Eq. (41) yields:

$$\begin{aligned}
\dot{V}_3 &\le -\sum_{i=1}^{i=3}\frac{k_i e_{1i}^2}{b_i^2 - e_{1i}^2} - \boldsymbol{e}_2{}^T\left(K_2 - \frac{1}{2}I\right)\boldsymbol{e}_2 + \frac{a}{\gamma}\left(-\boldsymbol{\theta}^T\boldsymbol{\theta} + \boldsymbol{\theta}^{*T}\boldsymbol{\theta}^*\right) + \frac{1}{2}\|\boldsymbol{\varepsilon}\|^2 + \frac{1}{4l}D^2 \\
&= -\sum_{i=1}^{i=3}\frac{k_i e_{1i}^2}{b_i^2 - e_{1i}^2} - \boldsymbol{e}_2{}^T\left(K_2 - \frac{1}{2}I\right)\boldsymbol{e}_2 + \frac{a}{\gamma}\left(-\boldsymbol{\theta}^T\boldsymbol{\theta} - \boldsymbol{\theta}^{*T}\boldsymbol{\theta}^*\right) + \frac{2a}{\gamma}\boldsymbol{\theta}^{*T}\boldsymbol{\theta}^* + \frac{1}{2}\|\boldsymbol{\varepsilon}\|^2 + \frac{1}{4l}D^2
\end{aligned} \tag{43}$$

Due to $\left(\boldsymbol{\theta}^* + \boldsymbol{\theta}\right)^T\left(\boldsymbol{\theta}^* + \boldsymbol{\theta}\right) \ge 0$, we can obtain:

$$-\boldsymbol{\theta}^{*T}\boldsymbol{\theta} - \boldsymbol{\theta}^T\boldsymbol{\theta}^* \le \boldsymbol{\theta}^{*T}\boldsymbol{\theta}^* + \boldsymbol{\theta}^T\boldsymbol{\theta} \tag{44}$$

Due to $\tilde{\boldsymbol{\theta}}^T\tilde{\boldsymbol{\theta}}=\left(\boldsymbol{\theta}^*-\boldsymbol{\theta}\right)^T\left(\boldsymbol{\theta}^*-\boldsymbol{\theta}\right)=\boldsymbol{\theta}^{*T}\boldsymbol{\theta}^*+\boldsymbol{\theta}^T\boldsymbol{\theta}-\boldsymbol{\theta}^{*T}\boldsymbol{\theta}-\boldsymbol{\theta}^T\boldsymbol{\theta}^*$, and using Eq. (44), we can obtain

$$-\boldsymbol{\theta}^{*T}\boldsymbol{\theta}^*-\boldsymbol{\theta}^T\boldsymbol{\theta}\le-\frac{1}{2}\tilde{\boldsymbol{\theta}}^T\tilde{\boldsymbol{\theta}} \tag{45}$$

Lemma 1 [Ren, Ge, Tee et al. (2010)]: For any positive constant vector $\boldsymbol{b}\in R^n$, the following inequality holds for any vector $\boldsymbol{x}\in R^n$ in the interval $|\boldsymbol{x}|<|\boldsymbol{b}|$: $\ln\frac{\boldsymbol{b}^T\boldsymbol{b}}{\boldsymbol{b}^T\boldsymbol{b}-\boldsymbol{x}^T\boldsymbol{x}}\le\frac{\boldsymbol{x}^T\boldsymbol{x}}{\boldsymbol{b}^T\boldsymbol{b}-\boldsymbol{x}^T\boldsymbol{x}}$.

Substituting Eq. (45) into Eq. (43) and using Lemma1, we have:

$$\begin{aligned}\dot{V}_3&\le-\sum_{i=1}^{i=3}\frac{k_ie_{1i}^2}{b_i^2-e_{1i}^2}-\boldsymbol{e}_2{}^T\left(K_2-\frac{1}{2}I\right)\boldsymbol{e}_2-\frac{a}{2\gamma}\tilde{\boldsymbol{\theta}}^T\tilde{\boldsymbol{\theta}}+\frac{2a}{\gamma}\boldsymbol{\theta}^{*T}\boldsymbol{\theta}^*+\frac{1}{2}\|\boldsymbol{\varepsilon}\|^2+\frac{1}{4l}D^2\\&\le-\rho V_3+C\end{aligned} \tag{46}$$

where $\rho=\min\left\{2\min\left(k_i\right),\frac{2\lambda_{\min}\left(K_2-\frac{1}{2}I\right)}{\lambda_{\max}\left(M\right)},a\right\},C=\frac{2a}{\gamma}\boldsymbol{\theta}^{*T}\boldsymbol{\theta}^*+\frac{1}{2}\|\boldsymbol{\varepsilon}\|^2+\frac{1}{4l}D^2$.

In order to ensure $\rho>0$, select $\min(k_i)>0,\lambda_{\min}(K_2-\frac{1}{2}I)>0$, where $\lambda_{\min}$ represents the minimum eigenvalue of the matrix, $\lambda_{\max}$ represents the maximum eigenvalue of the matrix. Multiplying the left and right sides of Eq. (46) by $e^{\rho t},t\ge0$, we can obtain:

$$\left(\dot{V}_3+\rho V_3\right)e^{\rho t}\le Ce^{\rho t},\quad\frac{d}{dt}\left(V_3e^{\rho t}\right)\le Ce^{\rho t} \tag{47}$$

Then take integrals on both sides：

$$V_3\le\left(V_3\left(0\right)-\frac{C}{\rho}\right)e^{-\rho t}+\frac{C}{\rho}\le V_3\left(0\right)+\frac{C}{\rho} \tag{48}$$

Define：

$$Q=2\left(V_3\left(0\right)+\frac{C}{\rho}\right) \tag{49}$$

According to the definition of V_3 and Eqs. (48)-(49),we can obtain：

$$\begin{aligned}&\frac{1}{2}\ln\frac{b_i^2}{b_i^2-e_{1i}^2}\le V_3\left(0\right)+\frac{C}{\rho},\|e_{1i}\|\le\sqrt{b_i^2\left(1-e^{-Q}\right)}\\&\frac{1}{2}\boldsymbol{e}_2{}^T\boldsymbol{M}_x\left(\boldsymbol{q}\right)\boldsymbol{e}_2\le V_3\left(0\right)+\frac{C}{\rho},\|e_{2i}\|\le\sqrt{\frac{Q}{\lambda_{\min}\left(\boldsymbol{M}_x\right)}}\\&\frac{1}{2\gamma}\tilde{\boldsymbol{\theta}}^T\tilde{\boldsymbol{\theta}}\le V_3\left(0\right)+\frac{C}{\rho},\|\tilde{\boldsymbol{\theta}}\|\le\sqrt{\gamma Q}\end{aligned} \tag{50}$$

Therefore, the errors of the closed-loop system e_{1i}, e_{2i}, $\tilde{\boldsymbol{\theta}}$ converge automatically to the compact sets Ω_{e_1} Ω_{e_2} $\Omega_{\tilde{\theta}}$, where $\Omega_{e_1} := \left\{ \boldsymbol{e}_1 \in R^n, \|e_{1i}\| \le \sqrt{b_i^2 \left(1 - e^{-Q}\right)} \right\}$,

$\Omega_{e_2} := \left\{ \boldsymbol{e}_2 \in R^n, \|e_{2i}\| \le \sqrt{\dfrac{Q}{\lambda_{\min}\left(\boldsymbol{M}_x\right)}} \right\}$, $\Omega_{\tilde{\theta}} := \left\{ \tilde{\boldsymbol{\theta}} \in R^n, \|\tilde{\boldsymbol{\theta}}\| \le \sqrt{\gamma Q} \right\}$.

Lemma 2 [Slotine and Li (1991)]: (Barbalat's lemma) A Lyapunov function candidate $V(x)$ is bounded if the initial condition $V(0)$ is bounded, $V(x)$ is positive definite and continuous, and if $\dot{V}(x) \le -\rho V(x) + C$, where $\rho > 0$ and $C > 0$.

From Lemma 2, we know that both the tracking errors of system states and estimation errors of uncertain parameters as well as unknown disturbance are bounded.

According to $\boldsymbol{F}_x = \boldsymbol{J}^{-T}(\boldsymbol{q})\boldsymbol{\tau}$, we can calculate the actual control torque. In a similar way, we can derive the dynamic equation of the outer frame and design the position controller.

5 Simulation

In this section, the simulation was carried out to illustrate the effectiveness of the proposed control scheme for the inspection robot with double frame.

In the simulation, the parameters of the inner frame for the robot are chosen as follows

$m_1 = 6kg$, $r_1 = 0.05m$, $L = 0.2m$, $\alpha = \pi/6$, $k = 1$.

The desired position trajectory in Cartesian space is set as $x_d = \begin{bmatrix} 1+0.5\sin(\pi/3*t) \\ 1+0.5\cos(\pi/3*t) \\ 1+0.5\sin(\pi/3*t) \end{bmatrix}$ m

The parameters of the controller are chosen as

$k_i = 10, K_2 = diag[100,100,100], b_i = 0.005$,

$\delta_i = 0.002, \boldsymbol{\Gamma} = \mathrm{diag}[150,150,150], l = 4$, γ=3, $a = 1.5$.

The friction force and external disturbances are given by

$\boldsymbol{F}_f(\dot{\boldsymbol{q}})$=0.3*sign$(\dot{\boldsymbol{q}})$N, $\boldsymbol{f}_{dis} = \begin{bmatrix} 0.15*\sin(t) + 0.12*\sin(1.15t + \pi/3) \\ 0.2*\sin(t) + 0.14*\sin(1.5t + \pi/6) \\ 0.12*\sin(t) + 0.13*\sin(1.5t + \pi/4) \end{bmatrix}$ N.

The position tracking curves of the aircraft skin inspection robot are shown in Fig. 4. Fig. 5 shows the tracking errors of position by using the sliding mode control and the backstepping control. As shown in Fig. 5, we know that there are lager errors by using sliding mode control, and it will cause the robot legs touch the surface of the aircraft skin. By using the backstepping control, there is a very small error in the system. Therefore, the latter is more suitable as a motion controller for the aircraft skin inspection robot. Fig. 6 shows the motor driving torque with the sliding mode control and the backstepping control. In Fig. 6, we know that sliding mode controller has great shaking, this will further affect the stability of adsorption. But the backstepping control does not cause

shaking phenomenon. Therefore, the backstepping controller can ensure the control torque is relatively smooth during the movement of the robot. Fig. 7 shows the approximation of unknown dynamics related with system states. Tab. 1 shows the comparison of the position tracking errors between sliding mode control and Backstepping control with output constraint.

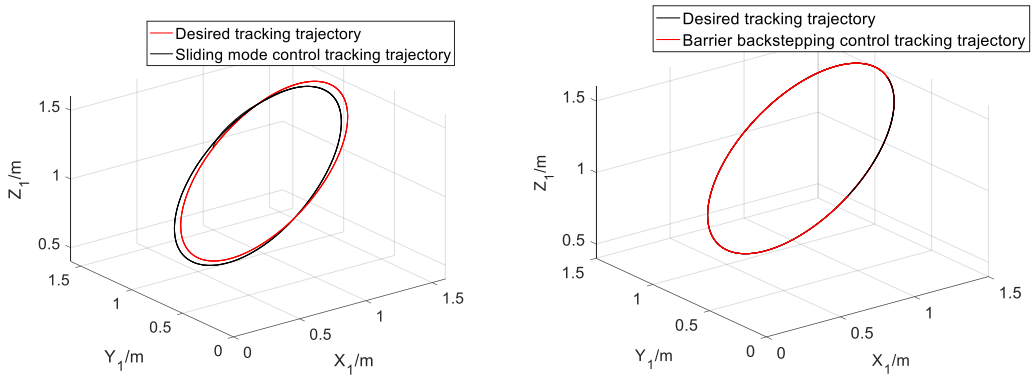

(a) Tracking trajectory with sliding mode control

(b) Tracking trajectory with backstepping control control

Figure 4: Tracking trajectories of the inspection robot

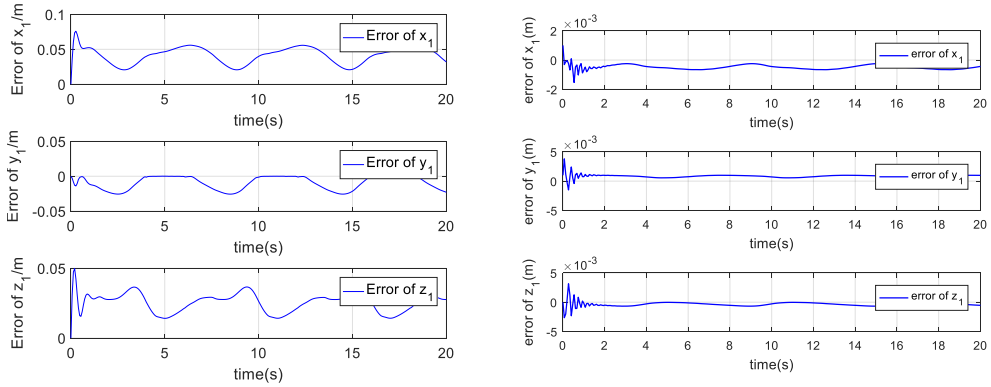

(a) Tracking errors of position with sliding mode control

(b) Tracking errors of position with backstepping control

Figure 5: Tracking errors of position

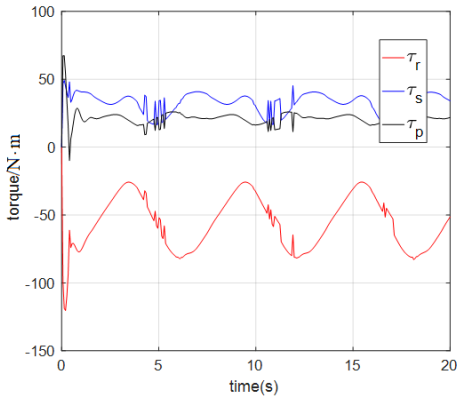

(a) Motor driving torques with sliding mode control

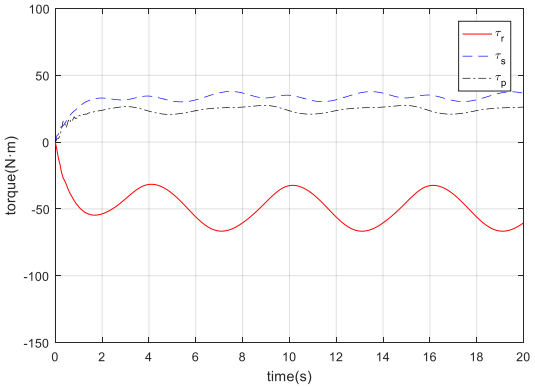

(b) Motor driving torques with backstepping control

Figure 6: Motor driving torques

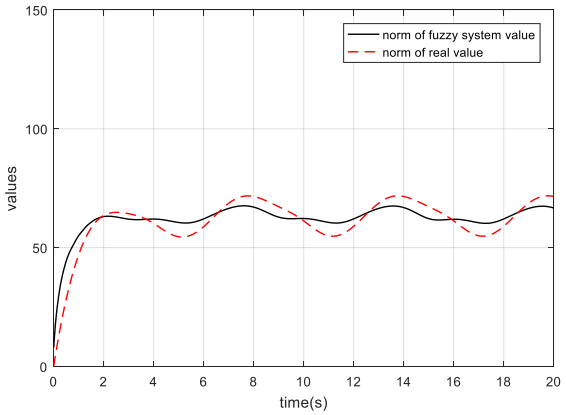

Figure 7: Approximation of the fuzzy system

Table 1: Position tracking errors

Range of Errors	Sliding mode control	Backstepping control with output constraint
Error of x1	(0,0.06) (m)	(-0.002,0.002) (m)
Error of y1	(-0.03,0) (m)	(-0.002,0.005) (m)
Error of z1	(0,0.04) (m)	(-0.003,0.004) (m)

6 Conclusion

In this paper, an improved aircraft skin inspection robot was introduced. First, the mechanical structure of the robot was described in detail. Second, the dynamic model of robot in Cartesian space was established and the motion control scheme based on the backstepping method using the barrier Lyapunov function for the aircraft skin inspection robot was designed. Considering the robot movement is restricted by the work environment,

the backstepping control method with output constraint is presented. The fuzzy system is adopted to approximate the unknown dynamics related with system states. Finally, the effectiveness of the control method is verified by simulation. Due to using the backstepping control, there is a very small error of trajectory tracking for the robot, and the control torque is relatively smooth during the movement of the robot. Therefore, the smooth motion of the robot can ensure the stability of the adsorption on the surface of aircraft.

Acknowledgement: This work was supported by the National Natural Science Foundation of China (Grant No. 61573185) and JiangSu Scientific Support Program of China (Grant No. BE2010190).

References

Apostolescu, T. C.; Alexandrescu, N.; Ionascu, G.; Bogatu, L. (2011): Design and control aspects of a climbing robot with vacuum cups attachment system. *Control Engineering & Applied Informatics*, vol. 13, no. 2, pp. 64-69.

Chen, M.; Ge, S. S.; How, B. V. E. (2010): Robust adaptive neural network control for a class of uncertain mimo nonlinear systems with input nonlinearities. *IEEE Transactions on Neural Networks*, vol. 21, no. 5, pp. 796-812.

Chen, M.; Ge, S. S.; Ren, B. (2011): Adaptive tracking control of uncertain mimo nonlinear systems with input constraints. *Automatica*, vol. 47, no. 3, pp. 452-465.

He, W.; Chen, Y.; Yin, Z. (2017): Adaptive neural network control of an uncertain robot with full-state constraints. *IEEE Transactions on Cybernetics*, vol. 46, no. 3, pp. 620-629.

He, W.; David, A. O.; Yin, Z.; Sun, C. (2015): Neural network control of a robotic manipulator with input deadzone and output constraint. *IEEE Transactions on Systems Man & Cybernetics Systems*, vol. 46, no. 6, pp. 759-770.

He, W.; Dong, Y.; Sun, C. (2015). Adaptive neural network control of unknown nonlinear affine systems with input deadzone and output constraint. *ISA Transactions*, vol. 58, pp. 96-104.

He, W.; Ge, W.; Li, Y.; Liu, Y. J.; Yang, C. et al. (2017): Model identification and control design for a humanoid robot. *IEEE Transactions on Systems Man & Cybernetics Systems*, vol. 47, no. 1, pp. 45-57.

He, W.; Li, Z.; Chen, C. L. P. (2017): A survey of human-centered intelligent robots: issues and challenges. *IEEE/CAA Journal of Automatica Sinica*, vol. 4, no. 4, pp. 602-609.

Yin, Z.; He, W.; Yang, C. (2015): Tracking control of a marine surface vessel with full-state constraints. *International Journal of Systems Science*, vol. 48, no. 3, pp. 535-546.

Yong, J.; Wang, H.; Fang, L.; Zhao, M. (2007): A novel approach to fault detection and identification in suction foot control of a climbing robot. *IEEE/RSJ International Conference on Intelligent Robots and Systems*, pp. 3423-3428.

Li, D. P.; Li, D. J.; Liu, Y. J.; Tong, S.; Chen, C. (2017): Approximation-based adaptive neural tracking control of nonlinear mimo unknown time-varying delay systems with full state constraints. *IEEE Transactions on Cybernetics*, vol.47, no. 10, pp. 3100-3109.

Li, Y.; Li, T.; Jing, X. (2014): Indirect adaptive fuzzy control for input and output constrained nonlinear systems using a barrier lyapunov function. *International Journal of Adaptive Control & Signal Processing*, vol. 28, no. 2, pp. 184-199.

Miyake, T.; Ishihara, H.; Shoji, R.; Yoshida, S. (2006): Development of small-size window cleaning robot by wall climbing mechanism. *ISARC Proceedings*.

Nagakubo, A.; Hirose, S. (1994): Walking and running of the quadruped wall-climbing robot. *IEEE International Conference on Robotics and Automation*, vol. 2, pp. 1005-1012.

Ngo, K. B.; Mahony, R.; Jiang, Z. P. (2005): Integrator backstepping using barrier functions for systems with multiple state constraints. pp. 8306-8312.

Niu, B.; Liu, Y.; Zong, G.; Han, Z.; Fu, J. (2017): Command filter-based adaptive neural tracking controller design for uncertain switched nonlinear output-constrained systems. *IEEE Transactions on Cybernetics*, pp. 1-12.

Niu, B.; Zhao, J. (2013). Tracking control for output-constrained nonlinear switched systems with a barrier lyapunov function. *International Journal of Systems Science*, vol. 44, no. 5, pp. 978-985.

Niu, B.; Zhao, J. (2013): Barrier lyapunov functions for the output tracking control of constrained nonlinear switched systems. *Systems & Control Letters*, vol. 62, no. 10, pp. 963-971.

Niu, B.; Zhu, J.; Su, Y.; Li, H.; Li, L. (2013): Tracking control of uncertain switched nonlinear cascade systems: a nonlinear h, ∞, sliding mode control method. *Nonlinear Dynamics*, vol. 73, no. 3, pp. 1803-1812.

Ren, B.; Ge, S. S.; Tee, K. P.; Tong, H. L. (2010): Adaptive neural control for output feedback nonlinear systems using a barrier lyapunov function. *IEEE Transactions on Neural Networks*, vol. 21, no. 8, pp. 1339-1345.

Ren,B.; Ge, S. S.; Tee, K. P.; Lee, T. H. (2010): Adaptive neural control for output feedback nonlinear systems using a barrier Lyapunov function. *IEEE Transactions on Neural Networks*, vol. 21, no. 8, pp. 1339-1345.

Rosa, G. L.; Messina, M.; Muscato, G.; Sinatra, R. (2002): A low-cost lightweight climbing robot for the inspection of vertical surfaces. *Mechatronics*, vol. 12, no. 1, pp. 71-96.

Slotine, J. E.; Li, W. (1991): *Applied Nonlinear Control*. Englewood Cliffs, NJ: Prentice-Hall.

Wettach, J.; Hillenbrand, C.; Berns, K. (2006): Thermodynamical modelling and control of an adhesion system for a climbing robot. *IEEE International Conference on Robotics and Automation*, pp. 2727-2732.

Zhang, H.; Zhang, J.; Zong, G. (2008): Effective pneumatic scheme and control strategy of a climbing robot for class wall cleaning on high-rise buildings. *International Journal of Advanced Robotic Systems*, vol. 3, no. 2.